State-resolved translation energy distributions for NCO photodissociation

Alexandra A. Hoops, Ryan T. Bise,[a] Jason R. Gascooke, and Daniel M. Neumark[b]
Department of Chemistry, University of California, Berkeley, California, 94720
and Chemical Sciences Division, Lawrence Berkeley National Laboratories, Berkeley, California 94720

(Received 30 January 2001; accepted 12 March 2001)

The photodissociation dynamics of NCO have been examined using fast beam photofragment translational spectroscopy. Excitation of the 1_0^2, 3_0^1, and $1_0^2 3_0^2$ transitions of the $\tilde{B}\,^2\Pi \leftarrow \tilde{X}\,^2\Pi$ band produces $N(^4S)+CO$ photofragments exclusively, while excitation of the $1_0^3 3_0^3$ transition yields primarily $N(^2D)+CO$ photoproducts. The translational energy $[P(E_T)]$ distributions yield $D_0(N\text{–}CO)=2.34\pm0.03$ eV, and $\Delta H_{f,0}^0(NCO)=1.36\pm0.03$ eV. The $P(E_T)$ distributions exhibit vibrationally resolved structure reflecting the vibrational and rotational distributions of the CO product. The $N(^2D)+CO$ distribution can be fit by phase space theory (PST), while the higher degree of CO rotational excitation for $N(^4S)+CO$ products implies that NCO passes through a bent geometry upon dissociation. The $P(E_T)$ distributions suggest that when the $\tilde{B}\,^2\Pi \leftarrow \tilde{X}\,^2\Pi$ band is excited, NCO undergoes internal conversion to its ground electronic state prior to dissociation. Excitation of NCO at 193 nm clearly leads to the production of $N(^2D)+CO$ fragments. While conclusive evidence for the higher energy $O(^3P)+CN(X\,^2\Sigma^+)$ channel was not observed, the presence of this dissociation pathway could not be excluded. © *2001 American Institute of Physics.* [DOI: 10.1063/1.1369132]

I. INTRODUCTION

The reaction dynamics of combustion intermediates have been investigated in many studies. Among the species examined, the NCO free radical has received considerable attention for its role as an intermediate in the combustion of nitrogenous fuels in air, whereby NO_x pollutants are released into the atmosphere. NCO has also been proposed as a key intermediate in the RAPRENO$_x$ (rapid reduction of NO_x) process, which serves to reduce the amount of NO_x from combustion exhausts.[1,2] This has stimulated much interest in the thermochemistry, spectroscopy, and photodissociation dynamics of NCO. In this work, we present results on the photodissociation of NCO that address these areas of interest.

Historically there has been some controversy over the value of the heat of formation of this free radical. Early determinations of $\Delta H_{f,0}^0(NCO)$ clustered around 1.6 eV.[3–5] A more direct measurement from the fast radical beam photodissociation experiments by Cyr *et al.*[6] yielded $\Delta H_{f,0}^0(NCO)=1.32\pm0.04$ eV. Corroboration of this lower value has come from subsequent theoretical[7] and experimental[8–10] investigations. However, a recent VUV photolysis study[11] has raised the issue again.

The spectroscopy of the ground and first two excited states of NCO has been studied by a variety of methods yielding vibrationally and rotationally resolved spectra. The first observation of the $\tilde{A}\,^2\Sigma^+ \leftarrow \tilde{X}\,^2\Pi$ and $\tilde{B}\,^2\Pi \leftarrow \tilde{X}\,^2\Pi$ transitions came in 1958 (Ref. 12) with analysis by Dixon in 1960.[13,14] Subsequently, there have been several investigations using absorption,[15,16] stimulated emission pumping,[17–19] and laser-induced fluorescence (LIF).[20–27] Additionally, the spectroscopy of the $\tilde{B}\,^2\Pi$ state was examined in the photodissociation experiments by Cyr *et al.*[6]

Several of these studies have also provided insight into the dynamical processes that NCO undergoes upon dissociation. Figure 1 illustrates the energy level diagram for NCO and its lowest energy fragmentation channels. In 1989, Liu and Coombe[5] investigated the photodissociation of NCO at 193 nm and observed $O(^3P)+CN(X\,^2\Sigma^+)$ products. Attempts to detect the $N(^2D)$ photofragment were unsuccessful, leading the authors to conclude that photolysis of NCO at 193 nm did not yield $N(^2D)$ as a major photoproduct. They observed a bimodal rotational distribution of the $CN(X\,^2\Sigma^+)$ photofragments; this distribution was interpreted as resulting from a bent excited dissociative state, yielding highly rotationally excited CN, and a linear bound excited state, generating CN products with little rotational excitation.

The work by Cyr *et al.*[6] in 1992 provided further insight into the dynamics of the dissociation of NCO. All vibrational levels of the $\tilde{B}\,^2\Pi$ state were found to predissociate to the following photoproducts:

$$NCO(\tilde{B}\,^2\Pi) \rightarrow N(^4S)+CO(X\,^1\Sigma^+), \quad (1)$$

$$NCO(\tilde{B}\,^2\Pi) \rightarrow N(^2D)+CO(X\,^1\Sigma^+). \quad (2)$$

The photofragment time-of-flight (TOF) distributions for both channels were fit using a vibrational distribution of the CO photofragments. Heats of reaction for the spin-forbidden channel (1) and the spin-allowed channel (2) were found to be 2.38 ± 0.04 and 4.76 ± 0.04 eV, respectively. Below the

[a]Current address: Lucent Technologies, Room 7C-227, 600-700 Mountain Ave., Murray Hill, New Jersey 07974.
[b]Author to whom correspondence should be addressed. Electronic mail: dan@radon.cchem.berkeley.edu

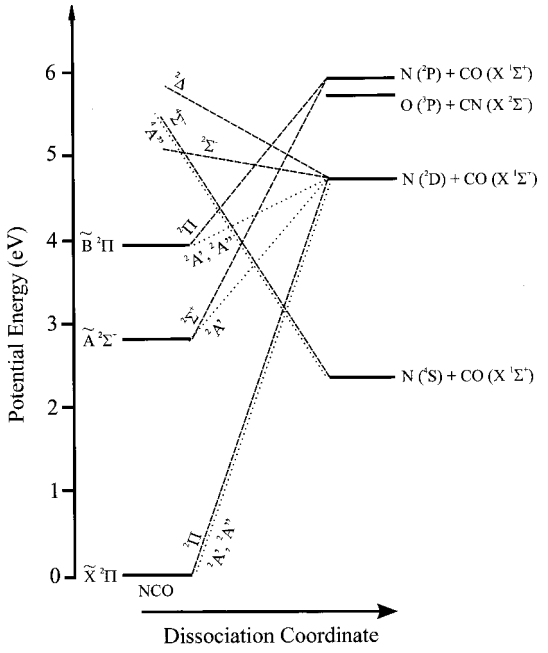

FIG. 1. Energy level diagram for the NCO free radical indicating the position of NCO electronic energy levels relative to the asymptotic energies of the fragment channels. Dashed and dotted lines indicate states adiabatically correlated in the linear and bent NCO geometries, respectively.

threshold for (2), NCO dissociates to $N(^4S)+CO(X\,^1\Sigma^+)$. However, once the spin-allowed channel becomes energetically accessible, virtually no channel (1) products are observed.

In this earlier study,[6] the spread in photofragment flight times was used to characterize the N+CO product energy distribution. In the work reported here, the dissociation dynamics from the NCO $\tilde{B}\,^2\Pi$ state were characterized using a photofragment coincidence detection scheme[28] that provides considerably better energy resolution than the original study. Structured photofragment translational energy distributions were obtained that allowed for evaluation of product branching ratios, vibrational and rotational distributions, and refined dissociation energies. Additionally, the dissociation of NCO at 193 nm was investigated in order to identify and characterize the nascent photofragments, including their degree of rotational and vibrational excitation.

II. EXPERIMENT

The experiments were performed on the fast beam photofragment translational spectrometer, Fig. 2. In this experiment, photodetachment of a mass-selected beam of precursor anions generates a clean source of neutral radicals, and these radicals are photodissociated by a second laser. As the instrument has been described in detail previously,[28–30] only a brief description will follow.

Rotationally and vibrationally cooled NCO^- is produced by bubbling neon (10 psig) through benzyl isocyanate (Aldrich) at room temperature, and then supersonically expanding the resulting gas mixture through a pulsed piezoelectric valve/electrical discharge source.[31] A 1 keV electron beam intersects the free jet expansion just downstream of the valve

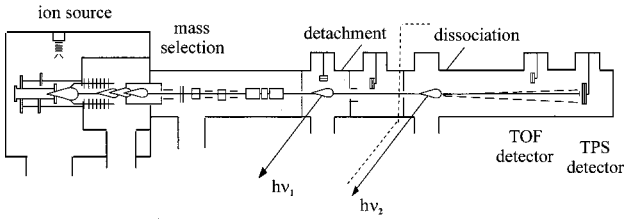

FIG. 2. Schematic diagram of the fast beam photofragment translational spectrometer. The dotted line divides the radical production region (left) from the photodissociation region (right).

orifice. The resulting molecular beam passes through a skimmer into a differentially pumped region, and anions in the beam are then typically accelerated to a laboratory beam energy of 8 keV, although energies as low as 5.5 keV can be used. NCO^- is mass selected using a Bakker time-of-flight (TOF) mass spectrometer, which imparts negligible kinetic energy spread to the ion beam.[32,33]

NCO^- is selectively photodetached by an excimer-pumped dye laser, and undetached ions are deflected out of the beam path. Based on the adiabatic electron affinity for NCO as determined in a previously reported photoelectron experiment of NCO^-,[34] a photodetachment energy of 3.66 eV was used to produce NCO exclusively in the $\nu_3=0$ level of the $\tilde{X}\,^2\Pi$ state for the majority of the experiments. Alternatively, the output of a XeCl excimer laser (4.03 eV) could be used for photodetachment in order to populate both the $\nu_3=1$ and $\nu_3=0$ vibrational levels of the ground electronic state of NCO. Based on peak intensities in the NCO^- photoelectron spectrum,[34] the population of $\nu_3=1$ level should be about $\frac{1}{2}$ that of the ground state at this higher detachment energy.

The radicals produced by photodetachment are then intersected by either the frequency doubled output of a second excimer-pumped dye laser with a bandwidth of 0.3 cm^{-1} tuned to a specific photon energy, or the output of an ArF excimer laser (193 nm). Resulting photofragments from a single parent molecule are detected directly by either the retractable TOF detector (see Fig. 2) or the time and position sensing (TPS) microchannel plate (MCP) detector assembly based on the concept developed by de Bruijn and Los.[35] The TPS detector yields the positions of both photofragments and difference in their arrival times; our implementation of this detector has been described in detail elsewhere.[28,29] An aluminum strip is placed across the center of the detectors in order to prevent undissociated parent radicals from striking the MCPs. Consequently, any observed signal is due to the recoiling photofragments.

Two types of experiments can be performed to characterize the photodissociation of NCO. First, the dissociation laser energy is scanned and the total flux of photofragments arriving at the TOF detector is measured, thereby producing photofragment yield (PFY) spectra. Second, the dissociation laser is tuned to specific photon energies, and dynamical information is obtained through the use of the TPS detector; for each dissociation event, the time and position information yields the masses of the fragments, their relative translational energy (E_T), and the polar angle θ between the relative ve-

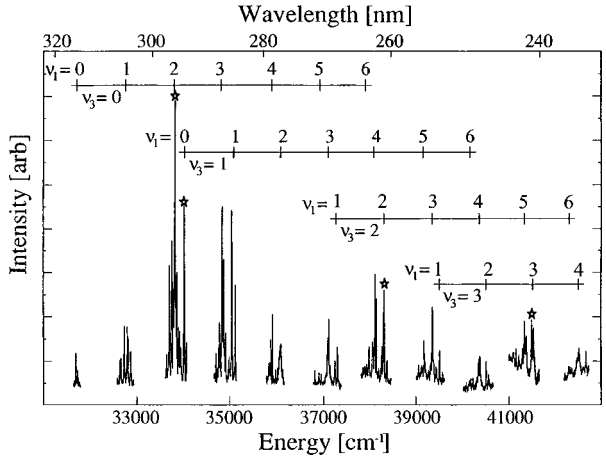

FIG. 3. NCO $\tilde{B}\,^2\Pi \leftarrow \tilde{X}\,^2\Pi$ photodissociation cross section from Ref. 6. Asterisks (*) indicate dissociation wavelengths at which $P(E_T)$ distributions were obtained.

locity vector and the electric vector of the polarized dissociation laser. The photofragment mass resolution is $m/\Delta m \approx 10$, while the translational energy resolution is $\Delta E_T/E_T = 2.2\%$.

The presence of a beam block across the center of the TPS detector reduces the acceptance of the detector for those fragments that are of low translational energy or have values of θ close to 0° or 180°, while fragments of high translational energy with θ close to 90° miss the detector entirely. These effects are accounted for by normalizing the raw translational energy distributions with a detector acceptance function (DAF),[28] and all data presented here have been corrected with the DAF.

III. RESULTS

A. Translational energy distributions, $\tilde{B}\,^2\Pi \leftarrow \tilde{X}\,^2\Pi$ transitions

The PFY spectrum for the $\tilde{B}\,^2\Pi \leftarrow \tilde{X}\,^2\Pi$ band of NCO is shown in Fig. 3. Peaks marked with an asterisk indicate the transitions at which $P(E_T)$ distributions were obtained. Photofragment coincidence experiments with the TPS detector were performed at photon energies of 4.20, 4.22, 4.76, and 5.15 eV, which correspond to the 1_0^2, 3_0^1, $1_0^2 3_0^2$, and $1_0^3 3_0^3$ transitions, respectively. The entire band in Fig. 3 lies below the threshold for dissociation to O+CN, 5.71 eV, as calculated with the use of the value of $\Delta H_{f,0}^0$(NCO) determined in this work (see Sec. IV).[36,37] Thus, N+CO is the only mass channel that needs to be considered. At each of the four transition energies, angle-independent translational energy distributions, $P(E_T)$, and energy-dependent anisotropy parameters, $\beta(E_T)$, were determined.[28]

$P(E_T)$ distributions for the 1_0^2, 3_0^1, and $1_0^2 3_0^2$ transitions are shown in Fig. 4. All of these measurements were taken with the TPS detector at a distance of 1 m from the photodissociation volume and with the laser polarization parallel to the radical beam axis. Only the spin-forbidden products, $N(^4S)+CO$, are accessible when these transitions are excited. The vertical dashed lines indicate the maximum translational energy (E_T^{max}) for $N(^4S)+CO$ at each excitation energy as determined by the analysis in Sec. IV. All three distributions extend to, but not beyond, this limit. The resolved structure apparent in these translational energy distributions consists of peaks spaced by approximately 270 meV, which corresponds to the frequency of the CO stretch. On average, the full width at half maximum (FWHM) of the resolved features is 220 meV with no significant variation in width with respect to either vibrational level or photon energy. However, there is more resolved structure at low E_T for the higher energy transitions. The vibrational and rotational distributions corresponding to these transitions are presented in Sec. IV.

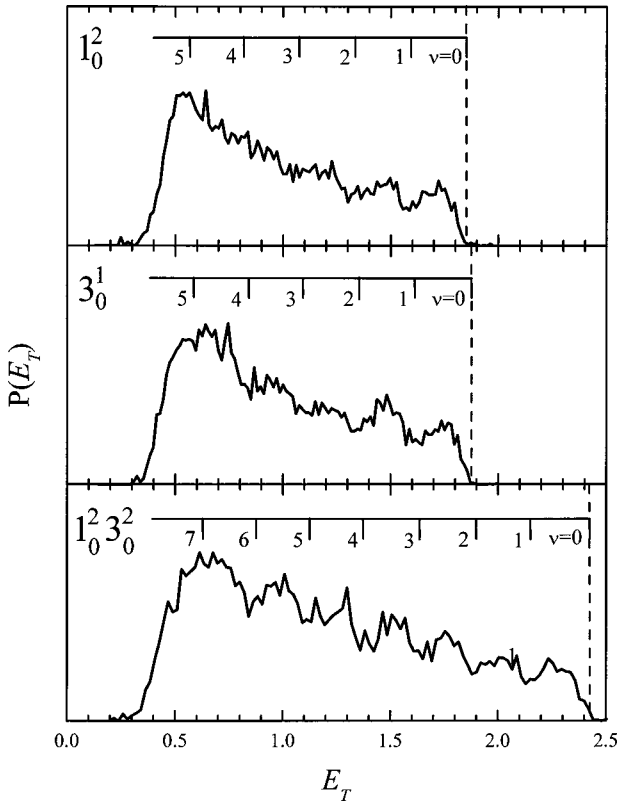

FIG. 4. $P(E_T)$ distributions for the N+CO channel resulting from 1_0^2, 3_0^1, and $1_0^2 3_0^2$ transitions of the $\tilde{B}\,^2\Pi \leftarrow \tilde{X}\,^2\Pi$ band. The vertical dashed lines indicate E_T^{max} for $N(^4S)+CO$ products.

At a photon energy of 5.15 eV ($1_0^3 3_0^3$ transition), dissociation to $N(^2D)+CO$ is possible. Figure 5 illustrates the $P(E_T)$ distribution at this photon energy taken at a 2 m flight length with the laser polarization parallel to the radical beam. At this flight length, the detector has a greater sensitivity to low translational energy fragments. Although this transition lies only 0.39 eV higher than the $1_0^2 3_0^2$ transition, the $P(E_T)$ distribution is very different. Virtually no signal is seen beyond $E_T = 0.43$ eV, which corresponds to E_T^{max} for $N(^2D)+CO$. Hence, the spin-allowed channel dominates once it becomes accessible, in agreement with the previous work by Cyr *et al.*[6] The $P(E_T)$ distribution exhibits two peaks separated by 270 meV, again corresponding to the CO stretch. The FWHM of these peaks is approximately 90 meV, substantially narrower than the peaks in Fig. 4. TPS data could

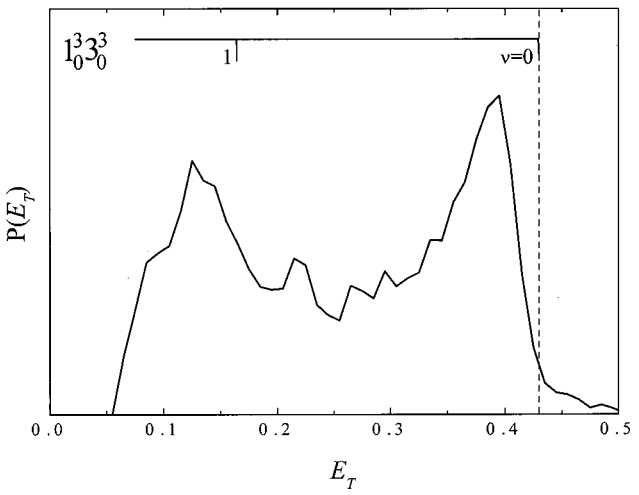

FIG. 5. $P(E_T)$ distributions for the N+CO channel resulting from the $1_0^3 3_0^3$ transition of the $\tilde{B}\,^2\Pi \leftarrow \tilde{X}\,^2\Pi$ band. The vertical dashed lines indicate $E_T^{\max}$ for the N(^2D)+CO fragments.

not be obtained for higher energy transitions of the $\tilde{B}\,^2\Pi \leftarrow \tilde{X}\,^2\Pi$ band due to low signal intensity.

Previously, Cyr *et al.*[6] found the spin-forbidden channel to have an anisotropy parameter of $\beta = +0.1$, with $\beta = +0.2$ for the spin-allowed channel. This is consistent with the current results. For both dissociation channels, the distributions were found to be nearly isotropic.

B. Translational energy distributions at 193 nm

$P(E_T)$ distributions for the photodissociation of NCO at 193 nm (6.42 eV) are shown in Fig. 6. The distributions displayed in Figs. 6(a) and 6(b) were taken at flight lengths of 1 and 2 m, respectively, with a detachment energy of 3.66 eV. In Fig. 6(c) the flight length was 2 m and the detachment energy was 4.03 eV, the latter resulting in some $\nu_3 = 1$ population of the NCO radicals (see Sec. II). The vertical dashed and dotted lines in Fig. 6 indicate $E_T^{\max}$ for the N(^2D)+CO and O(^3P)+CN($X\,^1\Sigma^+$) channels at 1.70 and 0.71 eV, respectively, assuming NCO is in its vibrational ground state.

The distributions in Fig. 6 were obtained assuming a 14:28 mass ratio, which corresponds to the N+CO mass channel. Measured mass distributions above and below the threshold for the O+CN mass channel do not exhibit any appreciable differences. Although the mass resolution of these experiments hinders the separation of the two mass channels, in previous studies of NCN and CNN we observed the presence of a N_2+C mass channel that was energetically overlapped with a CN+N mass channel.[38,39] A broadening and shifting of the peaks in the mass spectrum from those of a single channel marked the presence of both channels. A similar trend was not observed in the mass spectrum of the products of NCO photodissociation, indicating that the contribution from the O+CN mass channel is not substantially greater than the contribution from the N+CO mass channel in the region of $E_T \leqslant 0.71$ eV.

All of the signal at translational energies greater than 0.71 eV must be from N+CO, and the abrupt fall-off in signal above 1.70 eV indicates this to be N(^2D)+CO. A progression of peaks spaced by 270 meV with a FWHM of 220 meV is seen at high E_T in Fig. 6(a) and is assigned to the stretching vibration of the CO photofragment, since the O+CN channel is inaccessible in this translational energy range.

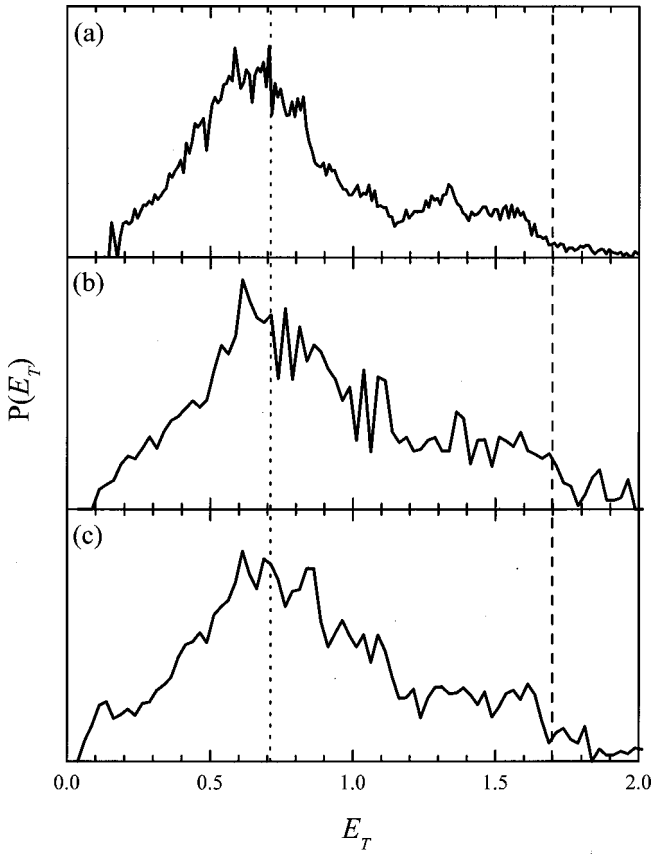

FIG. 6. $P(E_T)$ distributions for the dissociation of NCO at 193 nm. The flight lengths and photodetachment energies for these distributions are as follows: (a) 1 m, 3.66 eV; (b) 2 m, 3.66 eV; (c) 2 m, 4.03 eV. The vertical dashed and dotted lines indicate $E_T^{\max}$ for the N(^2D)+CO and O(^3P)+CN photoproducts, respectively.

Although there is increased intensity in the region near the energetic threshold for O(^3P)+CN($X\,^1\Sigma^+$) products, there is no clear feature that develops at the threshold that confirms the production of these photofragments. Extension of the flight length to 2 m to increase the sensitivity of the detector toward low translational energy fragments does not result in any changes in the product mass spectrum or $P(E_T)$ distribution [Fig. 6(b)]. Comparison of Figs. 6(b) and 6(c) shows that populating the $\nu_3 = 1$ level of NCO($\tilde{X}\,^2\Pi$) causes only minor differences in the $P(E_T)$ distribution, the most significant being a slight enhancement of signal below $E_T = 0.20$ eV in Fig. 6(c).

IV. ANALYSIS

A. Translational energy distributions, $\tilde{B}\,^2\Pi \leftarrow \tilde{X}\,^2\Pi$ transitions

Conservation of energy dictates that the photodissociation of NCO to N+CO mass fragments is described by

$$h\nu + E_{\text{int}}(\text{NCO}) = D_0(\text{N–CO}) + E_T + E_V(\text{CO}) + E_R(\text{CO}) + E_{\text{elec}}(\text{N}), \quad (3)$$

where $h\nu$ is the photon energy and E_{int}(NCO) is the average rotational energy of the parent radical. D_0(N–CO) is the bond dissociation energy, E_T is the measured center-of-mass translational energy, E_V(CO) is the vibrational energy of the CO fragment, E_R(CO) is the rotational energy of the CO fragment, and E_{elec}(N) is the atomic state energy of the nitrogen fragment. An equivalent equation can be written for the O+CN mass channel.

Based on a previous determination of the rotational temperature of NCO in the fast beam photofragment translational spectrometer,[6] a parent rotational temperature of 50 K was assumed in these experiments, corresponding to $E_{\text{int}}(\text{NCO}) = 0.004$ eV. Consequently, D_0 can be determined by finding the maximum translational energy, $E_T^{\max}$, of the photoproducts from the $P(E_T)$ distributions, at which point $E_V(\text{CO}) = E_R(\text{CO}) = 0$,

$$D_0(\text{N–CO}) = E_{h\nu} + 0.004\ \text{eV} - E_T^{\max} - E_{\text{elec}}(\text{N}). \quad (4)$$

Each distribution in Figs. 4 and 5 shows an abrupt onset of the dissociation signal so that the determination of $E_T^{\max}$, indicated by the dashed vertical lines, is relatively straightforward. The corresponding values for D_0(N–CO) agree within the experimental resolution of 30 meV, and the average of the values is $D_0 = 2.34 \pm 0.03$ eV. This represents a refinement of the dissociation energy previously determined by Cyr *et al.*,[6] 2.38 ± 0.04 eV, and is the value used in drawing the vertical dashed lines in Figs. 4–6.

The heat of formation of NCO can be calculated from this dissociation energy. Using the literature values of the heats of formation of atomic nitrogen and carbon monoxide,[36] $\Delta H_{f,0}^0$(NCO) was determined to be 1.36 ± 0.03 eV. This is within the error bars of the previous determination of $\Delta H_{f,0}^0(\text{NCO}) = 1.32 \pm 0.04$ eV by Cyr *et al.*,[6] and agrees with several other theoretical[7] and experimental[8,40] investigations. However, in a recent paper by Schönnenbeck and Stuhl,[11] in which VUV photolysis of NCO was monitored by emission from electronically excited CN products, evidence was presented for a lower limit of $\Delta H_{f,0}^0(\text{NCO}) \geqslant 1.72$ eV. The radicals in their experiment were produced by the F+HNCO reaction and were at room temperature or higher, which probably accounts for the discrepancy with our value as discussed previously.[6]

The translational energy distributions in Fig. 4 do not extend past $E_T^{\max}$ for N(^4S)+CO. However, the $P(E_T)$ distribution for the $1_0^3 3_0^3$ transition shows a small number of products beyond $E_T^{\max} = 0.43$ eV for N(^2D)+CO. Such fragments are likely due to the spin-forbidden pathway. Consequently, an upper limit on the branching ratio between the spin-allowed and spin-forbidden channels was obtained by assigning signal above and below 0.43 eV to N(^2D)+CO and N(^4S) photoproducts, respectively, yielding a branching ratio N(^2D):N(^4S)$\leqslant$96:4 for the $1_0^3 3_0^3$ transition.

The $P(E_T)$ distributions show resolved structure attributable to the vibration of the CO fragment. In order to determine the relative populations of the vibrational levels, each of the $P(E_T)$ distributions was fit to a series of distribution functions composed of Gaussians convoluted with a Boltzmann distribution. The details of this procedure have been described previously.[38] The resulting vibrational distributions are presented in Table I. Although vibrational levels beyond $\nu = 2$ for the 1_0^2 transition and $\nu = 3$ for the 3_0^1 transition are populated, the features were not of sufficient resolution to permit acceptable modeling by this method; Table I shows populations only for those vibrational levels that can be resolved. For the three $P(E_T)$ distributions in Fig. 4, all of the vibrational levels contribute between 10%–20% of the total distribution, with no apparent trends in vibrational population with excitation energy. The $1_0^3 3_0^3$ transition yields N(^2D)+CO products in which approximately twice as many of the CO fragments are in the $\nu = 0$ vibrational level as in the $\nu = 1$ level.

TABLE I. CO fragment vibrational distribution for transitions of the $\tilde{B}\,^2\Pi \leftarrow \tilde{X}\,^2\Pi$ band from a fit of the $P(E_T)$ distributions.

Transition	$\nu=0$ (%)	$\nu=1$ (%)	$\nu=2$ (%)	$\nu=3$ (%)	$\nu=4$ (%)	$\nu=5$ (%)
1_0^2	13	11	15			
3_0^1	11	11	13	15		
$1_0^2 3_0^2$	10	8	12	12	14	18
$1_0^3 3_0^3$	64	36				

The contours of the vibrational features reflect the rotational excitation of the CO photofragment. Thus, each vibrational feature can be evaluated in order to determine the rotational quantum number, N_{peak}, corresponding to the most populated CO rotational level. As shown in Table II, the values of N_{peak} for N(^4S)+CO fall in a narrow range, between 25 and 29, and appear to be independent of excitation energy and CO vibrational level. The blurring of resolved features at low E_T in Figs. 4(a) and 4(b) must reflect greater rotational excitation for the highly vibrationally excited CO products, but we cannot quantify this effect reliably. On the other hand, the $1_0^3 3_0^3$ transition leading to N(^2D)+CO photoproducts resulted in CO fragments with considerably less rotational excitation ($N_{\text{peak}} = 13$) in the two populated CO vibrational levels.

The measured $P(E_T)$ distributions were then compared to the translational energy distributions obtained from phase space theory (PST).[41] In this statistical theory, all product states allowed by conservation of energy and angular momentum are assumed to be equally probable. The details of determining translational energy distributions using PST have been described in detail previously.[42–44] Our application of PST assumes a long-range potential $V(r) = -C_0/r^6$, that the vibrational levels are described by the

TABLE II. Values of N_{peak} for the CO fragment vibrational features for transitions of the $\tilde{B}\,^2\Pi \leftarrow \tilde{X}\,^2\Pi$ band.

Transition	$\nu=0$	$\nu=1$	$\nu=2$	$\nu=3$	$\nu=4$	$\nu=5$
1_0^2	29	27	27			
3_0^1	25	25	27	27		
$1_0^2 3_0^2$	29	28	27	28	29	28
$1_0^3 3_0^3$	13	13				

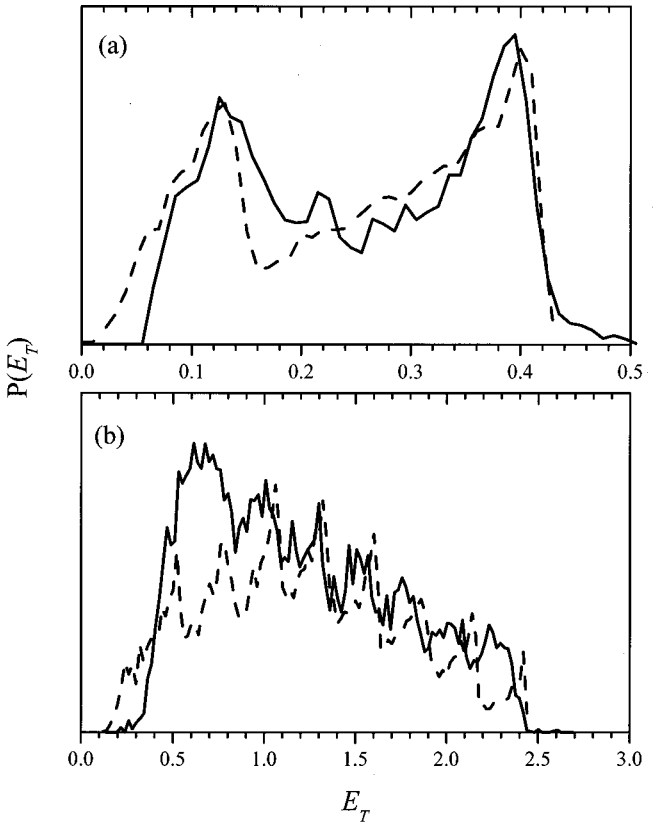

FIG. 7. Translational energy distributions for the (a) $1_0^3 3_0^3$ transition and (b) $1_0^2 3_0^2$ transition of the $\tilde{B}\,^2\Pi \leftarrow \tilde{X}\,^2\Pi$ band as measured experimentally (solid) and calculated from phase space theory (dashed).

harmonic oscillator approximation, and an initial parent temperature of 50 K. Finally, the calculated PST distributions have been convoluted with a Monte Carlo simulation program in order to account for the apparatus parameters.[28]

The translational energy distributions determined from PST are expected to agree with the measured $P(E_T)$ distributions if the dissociation process is barrierless and statistical. Furthermore, it is anticipated that the PST translational energy distributions for NCO will resemble those determined by Bonnet and Rayez[45] for the dissociation of the CCO radical as both radicals yield atoms of similar masses plus CO. As shown in Fig. 7(a), the $P(E_T)$ distribution for N(^2D) + CO resulting from the $1_0^3 3_0^3$ transition agrees well with the PST calculation. In contrast, there is a clear disparity between the PST calculation and the N(^4S) + CO distributions, as shown in Fig. 7(b) for the $1_0^2 3_0^2$ transition. The vibrational features in the experimental distribution show considerably more rotational excitation than in the PST calculation. These comparisons are discussed further in Sec. V.

B. Translational energy distributions, 193 nm dissociation

The $P(E_T)$ distributions at $h\nu = 6.42$ eV do not lend themselves to as thorough of an evaluation as those discussed above for the $\tilde{B}\,^2\Pi \leftarrow \tilde{X}\,^2\Pi$ band. The vertical dotted line at 0.71 eV denotes the expected $E_T^{\max}$ for the O(^3P) + CN($X\,^1\Sigma^+$) photoproducts. Due to the energetic overlap of the two mass channels and the lack of sufficient mass resolution, the O+CN mass channel could not be distinguished from the N+CO mass channel. An upper limit on the branching ratio between the O+CN and N+CO mass channels was determined by assigning intensity greater than 0.71 eV to N+CO and the remaining signal to O+CN. This yields (O+CN):(N+CO)$\leqslant$47:53. However, the discussion in the following section suggests that the O+CN yield is considerably less than this upper limit.

Determination of the relative vibrational populations was hindered by poorer resolution of discrete features in the $P(E_T)$ distributions. We were able to assign values of N_{peak} for $\nu = 0-2$ of the N(^2D) + CO channel, finding $N_{\text{peak}} = 28-30$. The amount of rotational excitation of the N(^2D) + CO products resulting from 193 nm excitation was greater than that of the same products from the $1_0^3 3_0^3$ transition and could not be suitably modeled by PST, indicating that the dissociation pathway for the two transitions is different.

V. DISCUSSION

The results from this experiment provide new insight into the dissociation mechanisms of NCO. The vibrationally resolved photofragment translational energy distributions reveal the extent of rotational excitation in the CO photoproducts. The products of the N(^2D) + CO channel have substantially lower rotational excitation than those of the N(^4S) + CO channel and the $P(E_T)$ distribution for the spin-allowed channel agrees with PST calculations. In contrast, the CO fragments associated with the N(^4S) + CO channel exhibit greater rotational excitation, and the photofragment translational energy distributions for this channel cannot be suitably modeled by PST.

Agreement between the measured $P(E_T)$ distribution for the N(^2D) + CO channel and that predicted by PST implies the absence of an exit barrier. The lack of such a barrier is also supported by the dominance of this channel as low as 0.1 eV above its energetic threshold.[6] These observations can be interpreted with reference to Fig. 1, which shows an adiabatic correlation diagram between NCO and various N+CO product channels for $C_{\infty v}$ (dashed lines) and C_s (dotted lines) symmetries.[5,46] For linear dissociation, the $\tilde{X}\,^2\Pi$ state of NCO correlates to N(^2D) + CO products, whereas the $\tilde{A}\,^2\Sigma^+$ and $\tilde{B}\,^2\Pi$ states correlate to higher energy N(^2P) + CO products. Although the $\tilde{A}\,^2\Sigma^+$ and $\tilde{B}\,^2\Pi$ states correlate to N(^2D) + CO in bent geometries, these dissociation pathways are likely to involve avoided crossings from higher lying NCO states, resulting in barriers with respect to N(^2D) + CO products. Hence, linear dissociation from the $\tilde{X}\,^2\Pi$ state appears to be the most plausible barrierless path to N(^2D) + CO products. Thus, we propose that these products are formed by internal conversion (IC) of NCO($\tilde{B}\,^2\Pi$) to the $\tilde{X}\,^2\Pi$ state followed by dissociation.

We next consider the mechanism for N(^4S) + CO production. Figure 1 shows that dissociation to these products can occur, in principle, by intersystem crossing (ISC) from the $\tilde{X}$, $\tilde{A}$, or $\tilde{B}$ states of NCO to the $^4\Sigma^-$($^4A''$) surface. However, the experimental observation that the spin-forbidden channel disappears as soon as the N(^2D) + CO

channel opens suggests that IC to the ground state occurs faster than any excited state dissociation processes regardless of whether the spin-allowed channel is accessible. If the spin-allowed channel is open, it is the dominant channel, and if not, $N(^4S)+CO$ is formed by ISC from the $\tilde{X}$ state. The substantial degree of rotational excitation we observe for the $N(^4S)+CO$ channel suggests that it involves passage over a barrier in a bent geometry.

An alternate dissociation mechanism for the spin-forbidden dissociation pathway has been suggested by Alexander and Werner.[46] Their calculations show that the $\tilde{B}\,^2\Pi$ and $\tilde{A}\,^2\Sigma^+$ states of NCO have a low energy conical intersection near the equilibrium geometry of the $\tilde{B}\,^2\Pi$ state. This crossing was found to lie energetically close to the minimum of the crossing between the $\tilde{A}\,^2\Sigma^+$ and $^4A''$ states, which occurs at a bent geometry of NCO with $\alpha=145.5°$. Therefore, they propose the following mechanism for the dissociation of NCO to spin-forbidden products:

$$NCO(\tilde{B}\,^2\Pi)\underset{IC}{\rightarrow}NCO(\tilde{A}\,^2\Sigma^+)\xrightarrow[ISC]{}NCO(^4A'')\rightarrow N(^4S)+CO. \quad (5)$$

This mechanism is likely to produce rotationally excited CO, as seen in the current experiments. However, in order to be consistent with our results, dissociation to $N(^2D)+CO$ must be significantly faster than the ISC step once this channel opens. This requires a barrierless pathway from the $\tilde{A}\,^2\Sigma^+$ state to these products, which seems unlikely based on the correlation diagram in Fig. 1. Nonetheless, it is certainly possible that IC to the $\tilde{X}$ state occurs sequentially through the $\tilde{A}\,^2\Sigma^+$ state, so that the crossing between the $\tilde{B}\,^2\Pi$ and $\tilde{A}\,^2\Sigma^+$ states plays an important role in the overall dynamics.

The work by Alexander and Werner points out that the energy of the $^4\Sigma^-(^4A'')$ state drops substantially upon bending. Hence, it would appear likely that the minimum crossing energy of this state with the $\tilde{X}$ state occurs at a bent geometry, as implied by the rotational distributions measured in our experiment for the $N(^4S)+CO$ channel. The simplest model one can apply to interpret these results is the modified impulsive model,[47,48] which predicts N_{peak} for each fragment vibrational state given the geometry at the barrier and the available energy. However, this model does not accurately describe the observed CO rotational excitation, as it predicts that N_{peak} decreases with increasing photofragment vibration, in contrast to our results (Table II).

The rotational reflection principle[49] provides a more sophisticated framework with which to interpret our results. In this model, the rotational distribution reflects a convolution of the bend wave function at the barrier with the final state interactions on the product side of the barrier (i.e., after ISC). Our observation that the values of N_{peak} for this channel are largely independent of photon energy and the CO vibrational quantum number suggests that (a) the bend wave function does not vary substantially over the range of energies probed in our experiment, and (b) product rotation and vibration are largely uncoupled by final state interactions. We should point out, however, that our determination of the CO rotational distribution is relatively crude; a more complete measurement using LIF or other rotationally resolved methods would provide significantly more insight into some of these issues.

Our results at 193 nm are of interest in light of the previous measurements of the photodissociation of NCO at this wavelength by Liu and Coombe,[5] who concluded that $O(^3P)+CN(X\,^2\Sigma^+)$ is the major dissociation channel through LIF detection of CN. No evidence of the $N(^2D)+CO$ channel was observed through either the use of resonance fluorescence to identify $N(^2D)$ or $N(^2P)$ atoms or measurement of NO β band emission following the interaction of $N(^2D)$ with N_2O. However, in our $P(E_T)$ measurements, the N+CO mass channel is clearly present, as we observe photofragment signal at translational energies that are inaccessible to O+CN products.

How can the markedly different results from the two experiments be explained? It is likely that in Liu and Coombe's experiment, the LIF detection of CN was more sensitive than the spectroscopic and chemical techniques used to identify $N(^2D)$. Similarly, our experiment cannot rule out the presence of some O+CN products. However, it is clear from the photofragment mass spectra that the O+CN mass channel is not the dominant channel at the translational energies detected in our work. We also considered the possibility that the O+CN products in Liu and Coombe's experiment arose from vibrationally excited NCO. Our $P(E_T)$ distribution in which a substantial fraction of the NCO was vibrationally excited [Fig. 6(c)] is not significantly different from that taken with vibrationally cold radicals [Fig. 6(b)], although there is slightly more signal at very low translational energies in Fig. 6(c).

A more quantitative comparison with the work of Liu and Coombe[5] can be made using their reported CN vibration-rotation distributions. They find a bimodal rotational distribution of the $CN(X\,^2\Sigma^+)$ products; the $CN(v=0)$ level is the most populated vibrational level for the high N products while the $CN(v=0)$ and $(v=1)$ levels with low N have nearly equal populations. The ratio of total high N to total low N products is 40:60. In our experiment, the most probable E_T for $CN(\nu=0)$ fragments with high N would be 0.20 eV, whereas $CN(\nu=0)$ photoproducts with low N would peak at $E_T=0.66$ eV. In Figs. 6(b) and 6(c), if we assign all of the signal below $E_T=0.20$ eV to O+CN (high N), and extrapolate to the amount of low N products using the results of Liu and Coombe, we calculate an upper limit of 4:96 for the (O+CN):(N+CO) branching ratio in Fig. 6(b) and 9:91 for Fig. 6(c). Given the observed $P(E_T)$ distributions, these are more realistic limits than that obtained by designating all the signal below 0.71 eV to O+CN, and provide further support for assigning O+CN as a minor channel at 193 nm.

VI. CONCLUSIONS

In the present work, the photodissociation dynamics of NCO following the 1_0^2, 3_0^1, $1_0^2 3_0^2$, and $1_0^3 3_0^3$ transitions of the $\tilde{B}\,^2\Pi\leftarrow\tilde{X}\,^2\Pi$ band were investigated using the technique of fast beam photofragment translational spectroscopy. At excitation energies $\leqslant 4.76$ eV, $N(^4S)+CO(X\,^1\Sigma^+)$ photoproducts were observed with CO rotational excitation consistent

with a dissociation mechanism that passes through a bent NCO geometry. An increase of the excitation energy to 5.15 eV resulted in the $N(^2D)+CO(X\,^1\Sigma^+)$ channel becoming the dominant pathway of dissociation. The degree of CO rotational excitation in these products was less than that of the spin-forbidden channel and could be modeled by phase space theory. These findings are consistent with a dissociation mechanism involving rapid IC from the $\tilde{B}$ to the $\tilde{X}$ state, followed by either (a) ISC to the $^4\Sigma^-(^4A'')$ surface and dissociation to $N(^4S)+CO$ products or (b) linear dissociation to $N(^2D)+CO$ products along a barrierless pathway. From the measured $P(E_T)$ distributions, the value of $D_0(N{-}CO)$ was directly determined to be 2.34 ± 0.03 eV, and $\Delta H^0_{f,0}(NCO)=1.36\pm0.03$ eV.

Photodissociation of NCO at 193 nm was also studied. The photofragment mass and $P(E_T)$ distributions show that $N(^2D)+CO$ is the dominant product channel at this wavelength; O+CN production appears to be at most a minor channel. It would clearly be of interest to perform experiments on NCO photodissociation at 193 nm and higher wavelengths using other product detection schemes such as laser-induced fluorescence or multiphoton ionization in order to corroborate the results reported here. In addition, the calculation of the potential energy surfaces and dissociation pathways for NCO should be a theoretically tractable problem, and we hope our work encourages efforts along these lines in order to provide a deeper understanding into the rich dynamics of this species.

ACKNOWLEDGMENTS

This research is supported by the Director, Office of Energy and Research, Office of Basic Energy Science, Chemical Sciences Division, of the U.S. Department of Energy under Contract No. DE-AC03-76F00098. We would also like to thank Dr. H. Choi for valuable advice on phase space theory, and Professor R. Coombe for discussions of his earlier work on NCO photodissociation.

[1] R. A. Perry and D. L. Siebers, Nature (London) **324**, 657 (1986).
[2] J. A. Miller and C. T. Bowman, Int. J. Chem. Kinet. **23**, 289 (1991).
[3] H. Okabe, J. Chem. Phys. **53**, 3507 (1970).
[4] B. J. Sullivan, G. P. Smith, and D. R. Crosley, Chem. Phys. Lett. **96**, 307 (1983).
[5] X. Liu and R. D. Coombe, J. Chem. Phys. **91**, 7543 (1989).
[6] D. R. Cyr, R. E. Continetti, R. B. Metz, D. L. Osborn, and D. M. Neumark, J. Chem. Phys. **97**, 4937 (1992).
[7] A. L. L. East and W. D. Allen, J. Chem. Phys. **99**, 4638 (1993).
[8] B. Ruscic and J. Berkowitz, J. Chem. Phys. **100**, 4498 (1994).
[9] S. S. Brown, H. L. Berghout, and F. F. Crim, J. Chem. Phys. **105**, 8103 (1996).
[10] M. Zyrianov, T. Drozgeorget, A. Sanov, and H. Reisler, J. Chem. Phys. **105**, 8111 (1996).
[11] G. Schönnenbeck and F. Stuhl, Chem. Phys. Lett. **264**, 199 (1997).
[12] R. Holland, D. W. G. Style, R. N. Dixon, and D. A. Ramsay, Nature (London) **182**, 337 (1958).
[13] R. N. Dixon, Can. J. Phys. **38**, 10 (1960).
[14] R. N. Dixon, Philos. Trans. R. Soc. London, Ser. A **252**, 165 (1960).
[15] D. E. Milligan and M. E. Jacox, J. Chem. Phys. **47**, 5157 (1967).
[16] P. S. H. Bolman, J. M. Brown, A. Carrington, I. Kopp, and D. A. Ramsay, Proc. R. Soc. London, Ser. A **343**, 17 (1975).
[17] F. J. Northrup, M. Wu, and T. J. Sears, J. Chem. Phys. **96**, 7218 (1992).
[18] M. Wu, F. J. Northrup, and T. J. Sears, J. Chem. Phys. **97**, 4583 (1992).
[19] M. Wu and T. J. Sears, Mol. Phys. **82**, 503 (1994).
[20] V. E. Bondybey and J. H. English, J. Chem. Phys. **67**, 2868 (1977).
[21] T. R. Charlton, T. Okamura, and B. A. Thrush, Chem. Phys. Lett. **89**, 98 (1982).
[22] K. N. Wong, W. R. Anderson, A. J. Kotlar, and J. A. Vanderhoff, J. Chem. Phys. **81**, 2970 (1984).
[23] R. A. Copeland and D. R. Crosley, Can. J. Phys. **62**, 1488 (1984).
[24] D. R. Woodward, D. A. Fletcher, and J. M. Brown, Mol. Phys. **62**, 517 (1987).
[25] D. Patel-Misra, D. G. Sauder, and P. J. Dagdigian, J. Chem. Phys. **93**, 5448 (1990).
[26] S. A. Wright and P. J. Dagdigian, J. Chem. Phys. **104**, 8279 (1996).
[27] J. L. Yao, J. A. Fernandez, and E. R. Bernstein, J. Chem. Phys. **107**, 8813 (1997).
[28] R. E. Continetti, D. R. Cyr, D. L. Osborn, D. J. Leahy, and D. M. Neumark, J. Chem. Phys. **99**, 2616 (1993).
[29] D. J. Leahy, D. L. Osborn, D. R. Cyr, and D. M. Neumark, J. Chem. Phys. **103**, 2495 (1995).
[30] D. L. Osborn, H. Choi, D. H. Mordaunt, R. T. Bise, D. M. Neumark, and C. M. Rohlfing, J. Chem. Phys. **106**, 3049 (1997).
[31] D. L. Osborn, D. J. Leahy, D. R. Cyr, and D. M. Neumark, J. Chem. Phys. **104**, 5026 (1996).
[32] J. M. B. Bakker, J. Phys. E **7**, 364 (1974).
[33] J. M. B. Bakker, J. Phys. E **6**, 785 (1973).
[34] S. E. Bradforth, E. H. Kim, D. W. Arnold, and D. M. Neumark, J. Chem. Phys. **98**, 800 (1993).
[35] D. P. de Bruijn and J. Los, Rev. Sci. Instrum. **53**, 1020 (1982).
[36] M. W. Chase and National Institute of Standards and Technology (U.S.), *NIST-IANAF Thermochemical Tables*, 4th ed. (American Chemical Society, American Institute of Physics for the National Institute of Standards and Technology, Washington, D.C., 1998).
[37] Y. H. Huang, S. A. Barts, and J. B. Halpern, J. Phys. Chem. **96**, 425 (1992).
[38] R. T. Bise, H. Choi, and D. M. Neumark, J. Chem. Phys. **111**, 4923 (1999).
[39] R. T. Bise, A. A. Hoops, H. Choi, and D. M. Neumark, J. Chem. Phys. **113**, 4179 (2000).
[40] M. Zyrianov, T. H. DrozGeorget, and H. Reisler, J. Chem. Phys. **106**, 7454 (1997).
[41] P. Pechukas and J. C. Light, J. Chem. Phys. **42**, 3281 (1965).
[42] P. Pechukas, J. C. Light, and C. Rankin, J. Chem. Phys. **44**, 794 (1966).
[43] P. J. Robinson and K. A. Holbrook, *Unimolecular Reactions* (Wiley–Interscience, New York, 1972).
[44] H. Choi, R. T. Bise, A. A. Hoops, D. H. Mordaunt, and D. M. Neumark, J. Phys. Chem. A **104**, 2025 (2000).
[45] L. Bonnet and J. C. Rayez, Chem. Phys. Lett. **296**, 19 (1998).
[46] M. H. Alexander and H.-J. Werner (private communication).
[47] G. Busch and K. Wilson, J. Chem. Phys. **56**, 3626 (1972).
[48] H. Levene and J. Valentini, J. Chem. Phys. **87**, 2594 (1987).
[49] R. Schinke, J. Chem. Phys. **85**, 5049 (1986).